Hindawi
Shock and Vibration
Volume 2021, Article ID 8552024, 11 pages
https://doi.org/10.1155/2021/8552024

Research Article

Research on Fault Extraction Method of CYCBD Based on Seagull Optimization Algorithm

Qianqian Zhang,[1] Haochi Pan,[2] Qiuxia Fan ,[1] Fujing Xu,[1] and Yulong Wu[1]

[1]*School of Automation and Software, Shanxi University, Taiyuan, Shanxi 030006, China*
[2]*School of Mechanical and Electrical Engineering, Guangdong University of Technology, Gangzhou, Gangdong 510006, China*

Correspondence should be addressed to Qiuxia Fan; fanqiuxia0808@126.com

Received 1 June 2021; Accepted 28 June 2021; Published 8 July 2021

Academic Editor: Liang Guo

Maximum cyclostationarity blind deconvolution (CYCBD) can recover the periodic impulses from mixed fault signals comprised by noise and periodic impulses. In recent years, blind deconvolution has been widely used in fault diagnosis. However, it requires a preset of filter length, and inappropriate filter length may cause the inaccurate extraction of fault signal. Therefore, in order to determine filter length adaptively, a method to optimize CYCBD by using the seagull optimization algorithm (SOA) is proposed in this paper. In this method, the ratio of SNR to kurtosis is used as the objective function; firstly, SOA is used to search the optimal filter length in CYCBD by iteration, and then it uses the optimal filter length to perform CYCBD; finally, the frequency-domain waveform is determined through Fourier transformation. The method proposed is applied to the fault extraction of a simulated signal and a test vibration signal of the closed power flow gearbox test bed, and the fault frequency is successfully extracted, in addition, using maximum correlation kurtosis deconvolution (MCKD) and multipoint optimal minimum entropy deconvolution adjusted (MOMEDA) to compare with CYCBD-SOA, which validated availability of the proposed method.

1. Introduction

The gearbox is widely used in the transmission system; fault diagnosis of the gearbox is necessary to ensure the safe and stable operation of the equipment [1, 2]. At present, scholars have put forward many methods to extract the fault signal in the mixed vibration signal. These methods include deep learning techniques [1–3], empirical mode decomposition (EMD) [4–6], ensemble empirical mode decomposition (EEMD) [7–9], local mean decomposition (LMD) [10], variational mode decomposition (VMD) [11–13], and blind deconvolution [14–16]. However, the forming process of rolling bearing fault source signal is a convolutional mixing process of source signal and noise, and the blind deconvolution can extract fault pulse through the deconvolution process, so the blind deconvolution has obvious advantage in bearing fault diagnosis [15].

At present, the fault diagnosis methods based on deconvolution theory include minimum entropy deconvolution (MED), maximum correlation kurtosis deconvolution (MCKD), multipoint optimal minimum entropy deconvolution adjusted (MOMEDA), and maximum cyclostationarity blind deconvolution (CYCBD). Wiggins first proposed the minimum entropy deconvolution method [17], and then many researchers applied MED to the field of fault diagnosis. Li et al. presented an improved MED which used the shuffled frog leaping algorithm to find the optimal filter coefficients, resulting in the accuracy of threshold selection being higher [18]. Cheng et al. adopted the standard particle swarm optimization algorithm to solve the filter coefficients of MED and successfully applied it to the fault signal extraction of railway bearings [19]. However, the limitation of MED is that it can deconvolve only a single impulse or a selection of impulses. In order to overcome the defects of the MED method, McDonald

et al. proposed the maximum correlated kurtosis deconvolution (MCKD) which enhances high correlated kurtosis and encourages periodicity about a specific period [20]. Wang et al. adopted the MCKD as the prefilter to denoise the vibration signals of heavy-load slewing bearing. Then, the intrinsic mode functions (IMFs) of the signals were decomposed by complementary ensemble empirical mode decomposition, and the optimal entropy values of IMFs were inputted into support vector machine. The fault feature extraction results of the practical combined failure signals were verified [21]. Zhang et al. employed MCKD to weaken the influence of the transmission path followed by TQWT, and then the signals were decomposed into multiple sub-bands in different Q values to enhance the fault features [22]. The number of shock pulses extracted by MCKD was increased, but only a limited number of shocks could be extracted locally. McDonald and Zhao proposed the multipoint optimal minimum entropy deconvolution adjusted (MOMEDA) which used a time objective vector to define the position and weight of the impulse sequence obtained by deconvolution, and the optimal filter can be solved without iterative algorithm [23]. Wang et al. used the grid search method to solve the optimal filter length of MOMEDA, and reliably applied it to extract the compound fault pulse signals in strong noise environment [24]. Li et al. proposed an algorithm based on the multipoint kurtosis spectrum characteristics and MOMEDA which adopted the spectrum fusion method to reconstruct the signal spectrum [25]. MOMEDA has a significant effect on the noise reduction, but it also greatly reduces the pulse amplitude in the vibration signal [15]. Buzzoni et al. proposed the maximum cyclostationarity blind deconvolution (CYCBD) which can well extract continuous periodic pulse and enhance the impact amplitude [14]. Chen et al. introduced the periodicity detection techniques (PDTs) to automatically identify the impulse period, and the PDT-assisted CYCBD can be enhanced bearing fault features with respect to CYCBD [26]. Wang et al. proposed a novel method that applied ACYCBD to obtain the deconvolution signal and then used instantaneous energy slice bispectrum (IESB) as a postprocessing method to suppress the residual noises [27]. Wang et al. proposed an adaptive method to determine the cyclic frequency set and filter length of CYCBD. The cyclic frequency set is determined by the autocorrelation function of morphological envelope, and the filter length is selected by the equal-step search strategy [15]. Compared with other deconvolution algorithms, CYCBD has better noise reduction performance, but the cyclic frequency and filter length have a great influence on it.

The seagull optimization algorithm (SOA) was put forward in 2019 by Dhiman and Kumar, and the test results prove that SOA acquired the competitive results compared with nine well-known optimization algorithms [28]. In this paper, the ratio of SNR to kurtosis is taken as the objective function, and SOA is used to adaptively select the filter length of CYCBD. The reliability of the combination of SOA and CYCBD is verified from the simulation signal and the experimental signal, respectively.

2. Basic Theory

2.1. Seagull Optimization Algorithm. The most important characteristics of seagulls are migration and aggressive behavior. Migration is the movement of animals from one place to another, according to the seasons in order to find the most abundant food sources and obtain enough energy. During migration, animals travel in groups. Each seagull is positioned differently during migration to avoid bumping into each other. In a group, seagulls can move in the direction of the best position. Seagulls often attack migratory birds forming a spiral movement pattern, as shown in Figure 1. The steps are as follows:

(1) Seagull population P_s parameter initialization: given the movement behavior of seagull in a given search space A, the behavior of B is randomized which is responsible for proper balancing between exploration and exploitation; the maximum number of iterations is $\mathrm{Max}_{\mathrm{iteration}}$; f_c is introduced to control the frequency of employing variable A which is linearly decreased from f_c to 0; $u$and v are constants to define the spiral shape.

$$A = f_c - \left(x * \left(\frac{f_c}{\mathrm{Max}_{\mathrm{iteration}}}\right)\right),$$
$$B = 2 * A^2 * r_d, \tag{1}$$

where $x = 0, 1, 2, \ldots, \mathrm{Max}_{\mathrm{iteration}}$, r_d is a random number which lies in the range of [0, 1].

(2) Calculation of the new search agent position to avoid the collision between neighbors, and movement towards best neighbor's direction:

$$\vec{C}_s = A \times \vec{P}_s(x), \tag{2}$$

$$\vec{M}_s = B \times \left(\vec{P}_{bs}(x) - \vec{P}_s(x)\right), \tag{3}$$

$$\vec{D}_s = \left|\vec{C}_s + \vec{M}_s\right|, \tag{4}$$

where $\vec{C}_s$ represents the position of search agent which does not collide with other search agents, $\vec{P}_s(x)$ represents the current position of the search agent, x indicates the current iteration, $\vec{M}_s$ represents the positions of the search agent $\vec{P}_s(x)$ towards the best fit search agent $\vec{P}_{bs}(x)$ (i.e., fittest seagull), and $\vec{D}_s$ represents the distance between the search agent and the best fit search agent.

(3) While attacking the prey, the spiral movement behavior occurs in the air. This behavior in x, y, z planes is described as follows. The best solution is calculated and saved and the position of other search agents is updated.

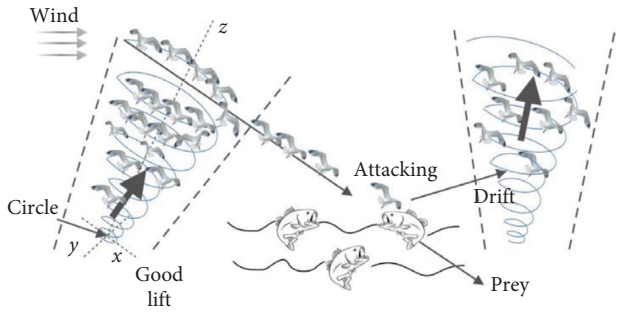

Figure 1: Migration and attacking behaviors of seagulls [28].

$$x' = r \times \cos(k), \tag{5}$$

$$y' = r \times \sin(k), \tag{6}$$

$$z' = r \times k, \tag{7}$$

$$r = u \times e^{kv}, \tag{8}$$

where r is the radius of each turn of the spiral, k is a random number in the range $[0 \le k \le 2\pi]$, and e is the base of the natural logarithm. The updated position of the search agent is calculated using equations (5)–(9).

$$\overrightarrow{P}_s(x) = \left(\overrightarrow{D}_s \times x' \times y' \times z'\right) + \overrightarrow{P}_{bs}(x), \tag{9}$$

where $\overrightarrow{P}_s(x)$ saves the best solution and updates the position of other search agents.

(4) Iterate from step (2) to step (3) to update the optimal solution until the maximum number of iterations.

2.2. CYCBD Algorithm. Generally, the purpose of blind deconvolution is to recover the source signal s_0 from the noise observation signal X, viz.,

$$\begin{aligned} s &= X * h \\ &= (s_0 * g) * h \approx s_0. \end{aligned} \tag{10}$$

The matrix form is as follows:

$$\begin{bmatrix} s[N-1] \\ \vdots \\ s[L-1] \end{bmatrix} = \begin{bmatrix} x[N-1] & \cdots & x[0] \\ \vdots & \ddots & \vdots \\ x[L-1] & \cdots & x[L-N-2] \end{bmatrix} \begin{bmatrix} h[0] \\ \vdots \\ h[N-1] \end{bmatrix}, \tag{11}$$

where g is the unknown impulse response function (IRF), h is the inverse filter, s is the estimated input, and $*$ refers to the convolution operation, and L and N are the total samples of s and h, respectively.

In reference [14], cyclic frequency of a discrete-time signal is defined as

$$\alpha = \frac{k}{T_s}, \tag{12}$$

where k is the sample index and T_s is the period (in the sample), which can be related to the failure rate.

The second-order cyclostationarity (ICS_2) is defined as follows:

$$\mathrm{ICS}_2 = \frac{\sum_{k>0} \left|c_s^k\right|^2}{\left|c_s^0\right|^2}, \tag{13}$$

with

$$c_s^k = \frac{E^H |s|^2}{L-N+1}, \tag{14}$$

$$c_s^0 = \frac{s^H s}{L-N+1}, \tag{15}$$

where

$$\begin{aligned} |s|^2 &= \left[|s[N-1]|^2, \ldots, |s[L-1]|^2\right]^T, \\ E &= [e_1 \ldots e_k \ldots e_K], \\ e_k &= \begin{bmatrix} e^{-j2\pi\left(k/T_s\right)}(N-1) \\ \vdots \\ e^{-j2\pi\left(k/T_s\right)}(L-1) \end{bmatrix}. \end{aligned} \tag{16}$$

According to (14) and (15), (13) can be expressed as

$$\mathrm{ICS}_2 = \frac{|s|^{2H} E E^H |s|^2}{\left|s^H s\right|^2}. \tag{17}$$

In this case, the signal containing the periodic component $|s|^2$ is called $\mathrm{P}[|s|^2]$, which contains all the interested periodic frequencies k, and can be written as

$$\mathrm{P}\left[|s|^2\right] = \frac{1}{L-N+1} \sum_k e_k \left(e_k^H |s|^2\right) = \frac{E E^H |s|^2}{L-N+1}. \tag{18}$$

Bringing (10) and (18) into (17) gives the following formula:

$$\mathrm{ICS}_2 = \frac{h^H X^H W X h}{h^H X^H X h}, \tag{19}$$

where h is the inverse filter; the weighting matrix W can be expressed as

$$\begin{aligned} W &= \mathrm{diag}\left(\frac{\mathrm{P}|s|^2}{s^H s}\right)(L-N+1) \\ &= \begin{bmatrix} \ddots & & 0 \\ & P\left[|s|^2\right] & \\ 0 & & \ddots \end{bmatrix} \frac{(L-N+1)}{\sum_{l=N-1}^{L-1} s^2}. \end{aligned} \tag{20}$$

According to (19) and (20), the shock source with the largest ICS_2 behavior can be extracted.

2.3. CYCBD Based on the Seagull Optimization Algorithm. Seagull optimization algorithm has a simple program, which can not only obtain the global optimal solution but also has high search precision and efficiency. The objective function is established and the seagull optimization algorithm is used to find the optimal filter length of CYCBD. Generally, the larger the SNR of the periodic fault pulse signals in the background of strong noise is, the better it is. For the kurtosis, if the signal fluctuates gently and contains several impulses, the kurtosis value is large. If the signal contains continuous pulses, the more the number of pulses, the smaller the corresponding kurtosis value. Therefore, the SNR is taken as the numerator and the kurtosis as the denominator to establish the objective function and can be written as

$$F = \frac{\text{SNR}}{\text{kurtosis}}. \tag{21}$$

That is, when the objective function value is the maximum, the corresponding filter length is the optimal solution. The flow chart of the proposed method is shown in Figure 2.

3. Simulation Analysis

3.1. Effects of Filter Lengths L on CYCBD. To illustrate the effect of L on the CYCBD results, a simulated signal y is constructed, as shown in formula (22). The signal consists of periodic pulses and random noise:

$$y = A_1 e^{-g\times 2\pi f_n t} \times \sin\left(2\pi f_n t \times \sqrt{1-g^2}\right) + 0.5 \times \zeta, \tag{22}$$

where the nature frequency $f_n = 50$, damping coefficient $g = 0.1$, and amplitude $A_1 = 1.5$.

The waveform of the signal is shown in Figure 3.

Figure 3 shows the time-domain graph of the simulated signal. Figure 3(a) is the fault impulse signal, and Figure 3(b) is the composite signal after adding noise. It can be observed that the periodic impact (Figure 3(a)) is submerged by noise.

CYCBD recovers the fault source by solving a finite length filter to perform the deconvolution and extract the continuous periodic pulse well. However, the filter length has a great influence on the noise reduction results. In order to illustrate the influence of the filter length on CYCBD results, the different filter lengths ($L = 200$, 400, 600, and 800) were used to denoise the simulation signal y. The frequency corresponding to the fault period of the simulation signal is 50 Hz. Referring to [14], the cycle frequency set is set as [50, 100, 150, 200, 250, 300, 350, 400, 450, 500]. Figure 4 shows the processing results of CYCBD with different filter lengths. The left side is the time-domain waveform after noise reduction, and the right side is the frequency-domain waveform after FFT.

It can be obviously seen from Figure 4 that different filter lengths have a great influence on the noise reduction results and periodic pulse extraction of CYCBD. When $L = 200$, the result denoised by CYCBD contains a large amount of noise, and there are individual pulses in the corresponding frequency-domain waveform. However, the pulse frequencies are 19.99 Hz, 79.96 Hz, 119.9 Hz, 179.9 Hz, and 219.9 Hz. There is no fault frequency and its frequency doubling. When $L = 400$, the noise amplitude decreases and more pulses appear in the frequency-domain waveform, but the pulse frequencies are 39.98 Hz, 59.96 Hz, 89.94 Hz, 109.9 Hz, 139.9 Hz, etc.; the signal mixing phenomenon still exists. When $L = 600$, the noise amplitude is greatly reduced, and the continuous periodic pulses can be observed in the time domain. The fault frequency of 50 Hz and its multiples are uniformly distributed in the frequency-domain waveform. When $L = 800$, the signal extracted by CYCBD is distorted, and no protruding pulse appears in the frequency-domain waveform. The results show that if the filter length is not properly selected, CYCBD cannot effectively extract the periodic pulse submerged by noise.

3.2. Adaptive Determination of the Optimal Filter Length. In order to find the optimal filter length adaptively, the seagull optimization algorithm is used to search the optimum solution. The less the noise contained in the signal, the greater the SNR value. The larger the number of periodic pulses extracted, the smaller the kurtosis value. Therefore, the objective function value is taken as the optimization objective to find the filter length corresponding to the maximum.

The method proposed in this paper is used to extract the fault signal from the simulation signal in Section 3.1. The optimal filter length obtained by the SOA is 499, and the corresponding CYCBD result is shown in Figure 5. The results show that the fault signals with fault frequencies of 50 Hz and its multiples can be extracted effectively.

4. Experimental Verification

4.1. Test Bench. In order to verify the practicability of CYCBD-SOA in the fault features extraction of the outer ring of the rolling bearing, a closed power flow gearbox test bench was used to carry out the relevant tests. The vibration signals of the outer ring faults were collected. The closed power flow test bench is loaded by the internal force generated by the torsion bar, and the speed is adjusted by the electromagnetic speed-regulating asynchronous motor with a range of 0 r/min–1500 r/min. The gearbox test bench is shown in Figure 6. The type of the piezoelectric sensor is CA-YD-186 with a sensitivity of 10.41 mv/m $\cdot$ $s^{-2}$and a sampling frequency of 12000 Hz. The tapered roller bearings, type is 32212, are arranged on a side of the headstock driving wheel away from the coupling. The bearing with outer ring cracks was used to replace the healthy bearing, as shown in Figure 7. The crack of the outer ring is formed by the electrical spark machining, as shown in Figure 8. After calculation, the instantaneous frequency of bearing outer ring is $f = 4.73 f_r$, where f_r is the rotational frequency of the rotating shaft.

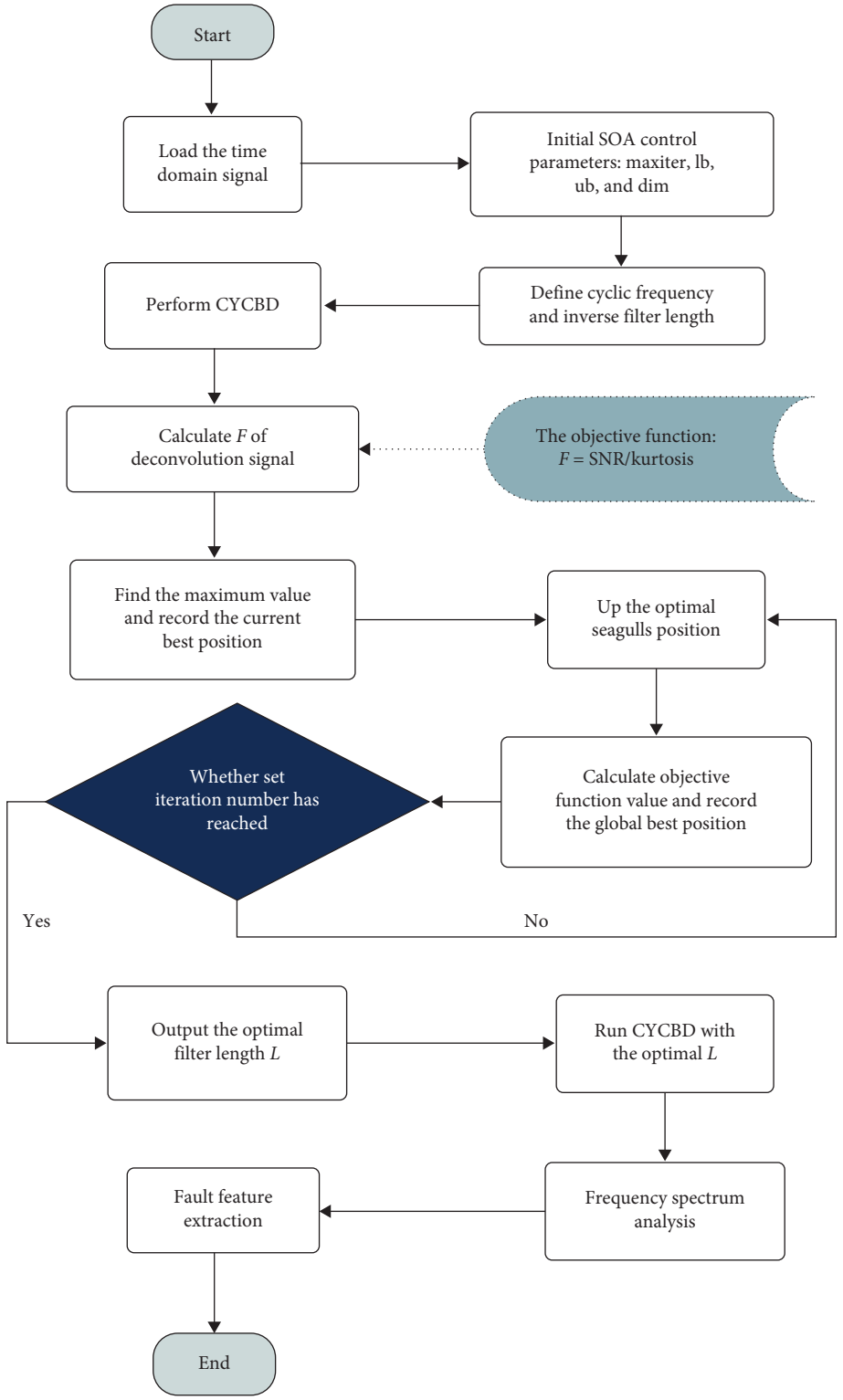

Figure 2: Flow chart of the proposed method.

4.2. Comparison and Analysis. In the test, the sampling frequency is 12000 Hz and the rotating speed is 510 r/min. After calculation, the fault frequency of the outer ring is 40 Hz. The vibration signals collected are shown in Figure 9. Due the noise is too large, the periodic pulse cannot be observed in the time-domain waveform, and the fault features in the frequency-domain waveform are not obvious.

Referring to [14], the cycle frequency set is set as [40, 80, 120, 160, 200, 240, 280, 320, 360, 400]. The vibration signals obtained from the tests were denoised by CYCBD-SOA. The

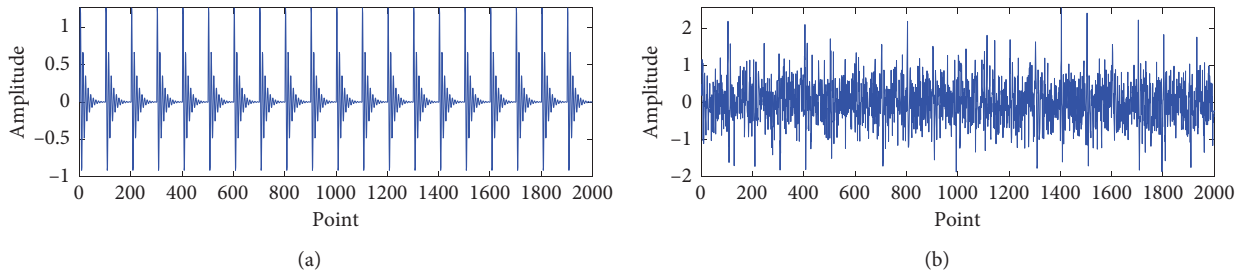

Figure 3: Simulated signal.

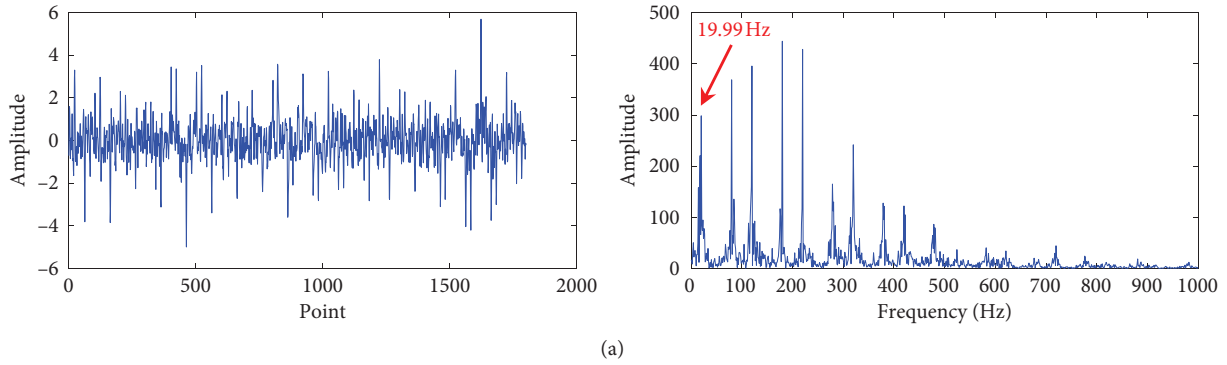

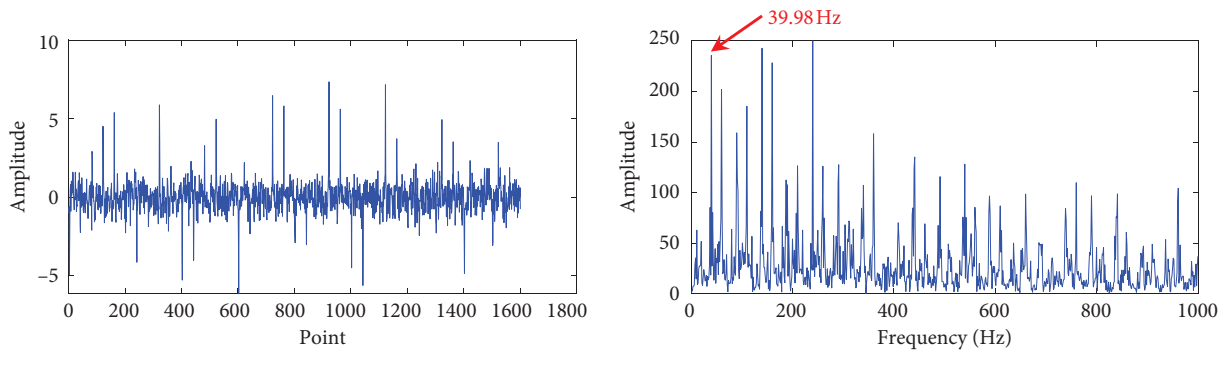

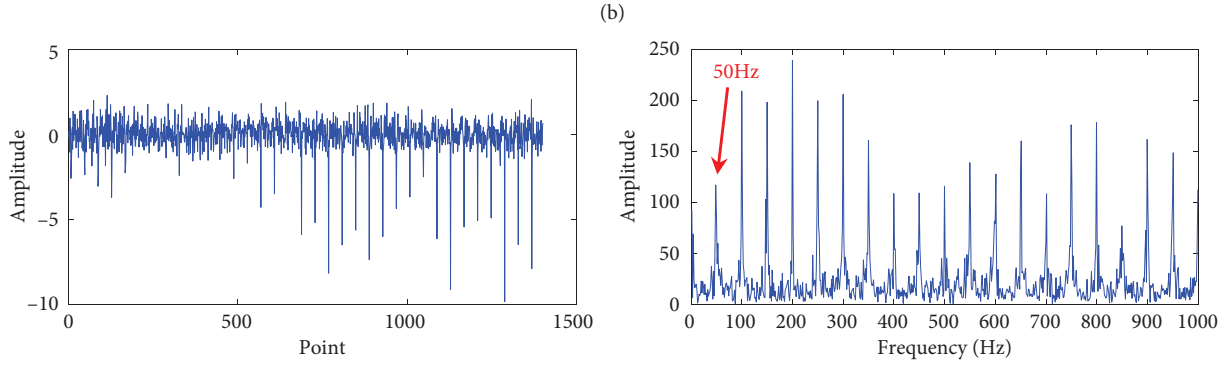

Figure 4: Continued.

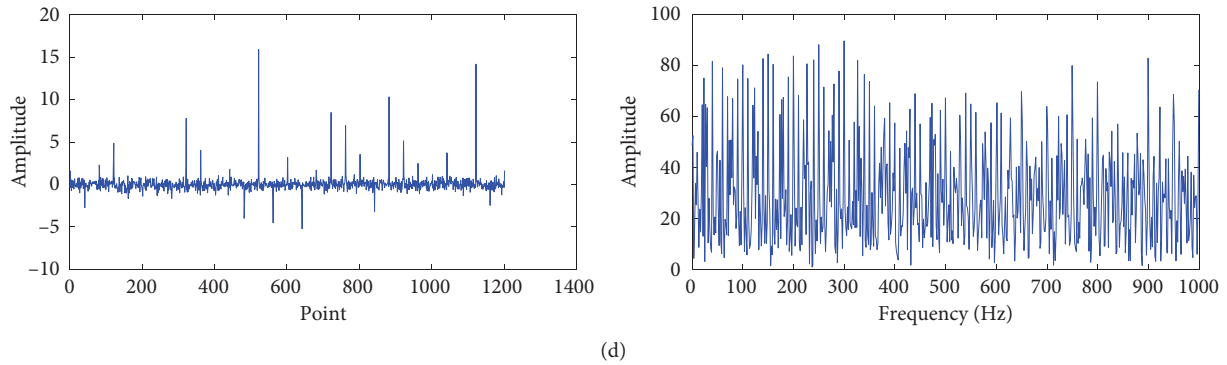

Figure 4: Results of CYCBD with different filter lengths L: (a) $L = 200$, (b) $L = 400$, (c) $L = 600$, and (d) $L = 800$.

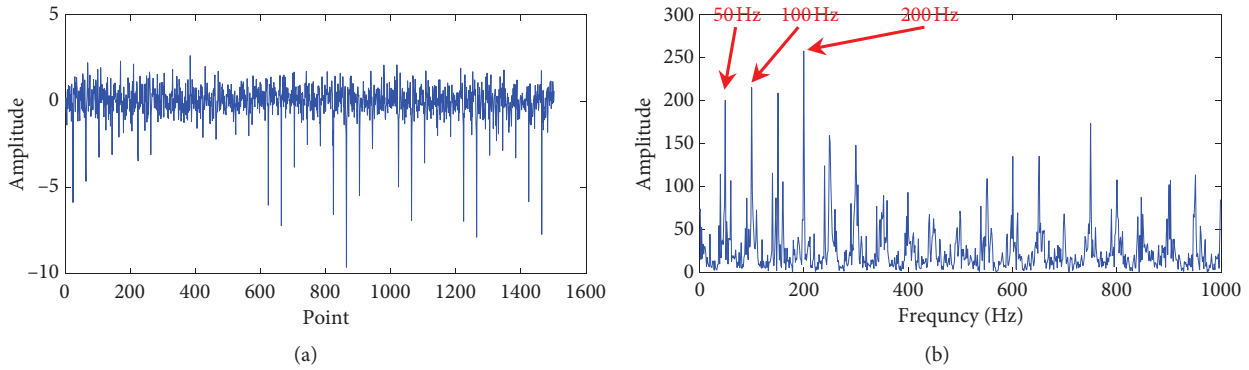

Figure 5: Results of ACYCBD: (a) time-domain waveform and (b) frequency-domain waveform.

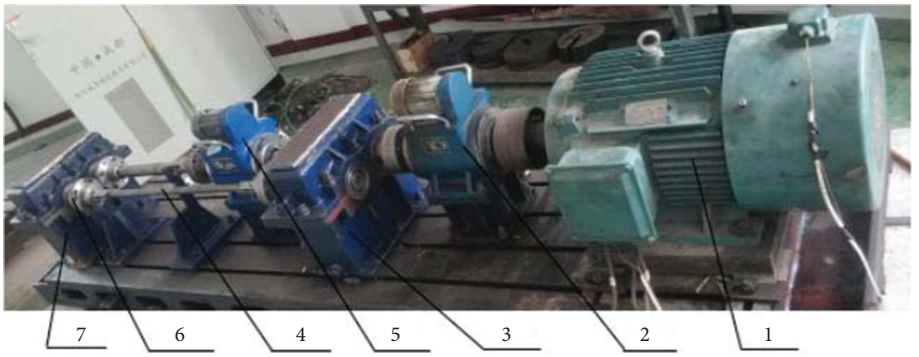

Figure 6: The gearbox test bench. 1, speed-regulating motor. 2, coupling. 3, gearbox. 4, torsion bar. 5, torque tachometer. 6, piezoelectric acceleration sensor. 7, test gearbox.

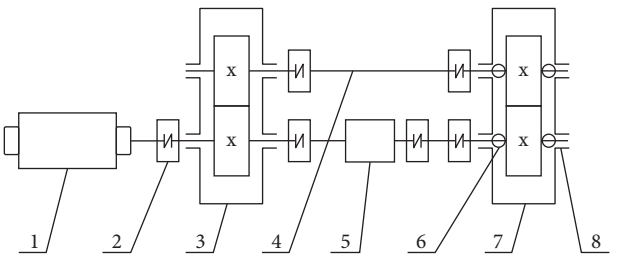

Figure 7: Schematic diagram of the test bed structure. 1, speed-regulating motor. 2, coupling. 3, gearbox. 4, torsion bar. 5, torque tachometer. 6, piezoelectric acceleration sensor. 7, test gearbox. 8, test bearing.

Figure 8: The crack fault of bearing outer ring.

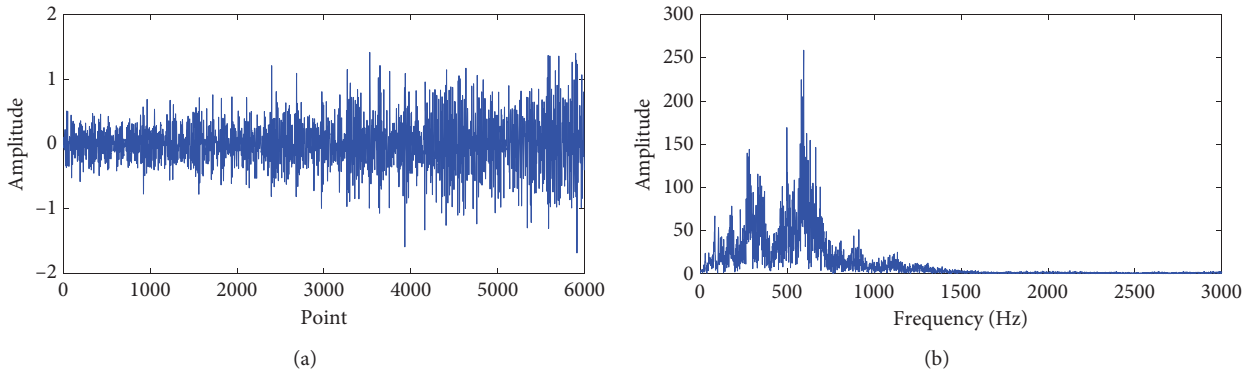

Figure 9: Experimental fault signal: (a) time-domain waveform and (b) frequency-domain waveform.

calculated optimal filter length is 499, and the corresponding CYCBD-SOA result is shown in Figure 10. It can be seen from the time-domain waveform that the noise component is greatly reduced, and the fault pulse is prominent in the frequency-domain waveform. There are 24 obvious peaks at 50 Hz and its integer multiples, and the frequency cluster reaches to 980 Hz. Therefore, the CYCBD-SOA can successfully extract the fault frequency of the outer ring faults.

To illustrate the superiority of CYCBD-SOA, the test vibration signal was processed with MCKD and MOMEDA. The results obtained by the three methods mentioned above are compared and analyzed.

MCKD is used to process the test vibration signal. The filter length is set to 600 and the deconvolution period is 50. The results of MCKD are shown in Figure 11. It can be seen from the time-domain waveform that the noise is weakened and the fault pulse is prominent. There are 24 continuous periodic pulses with frequencies of 38.3 Hz, 81 Hz, 123 Hz, 202.3 Hz, 240.3 Hz, and so on, in the frequency-domain waveform. The extracted fault frequency is close to 40 Hz and its integer multiples, but exists in some deviations. In addition, the amplitude of the fault frequency extracted by MCKD is small; it is easy to be submerged by the strong noise signal.

The filter length is set as 600 and the period is 50. MOMEDA is used to process the test vibration signal. The results are shown in Figure 12. The time-domain waveform shows that the noise is attenuated. For the frequency-domain waveform, it can be observed that there are 24 continuous pulses at 39.2 Hz, 81 Hz, 120 Hz, 162 Hz, 200 Hz, and so on. Compared with MCKD, the extraction accuracy of fault frequency is improved and the amplitude is strengthened.

Therefore, the comparative analysis of the results obtained by the three deconvolution methods shows that CYCBD-SOA has obvious advantages. It can extract the continuous periodic pulses accurately and enhance the

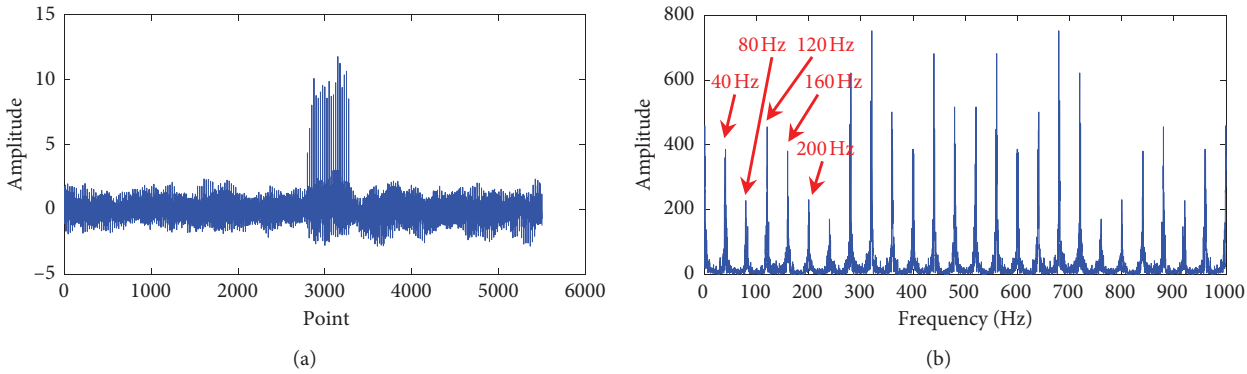

Figure 10: Results of CYCBD-SOA: (a) time-domain waveform and (b) frequency-domain waveform.

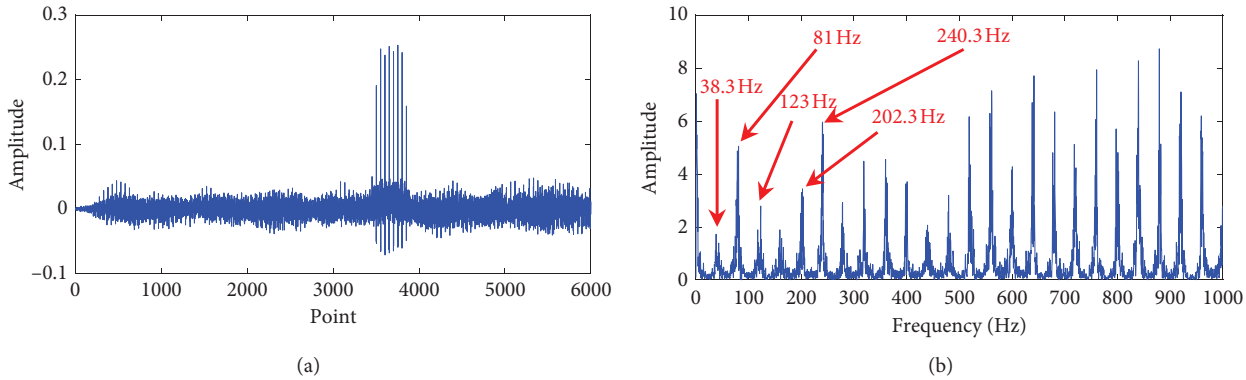

Figure 11: Results of MCKD: (a) time-domain waveform and (b) frequency-domain waveform.

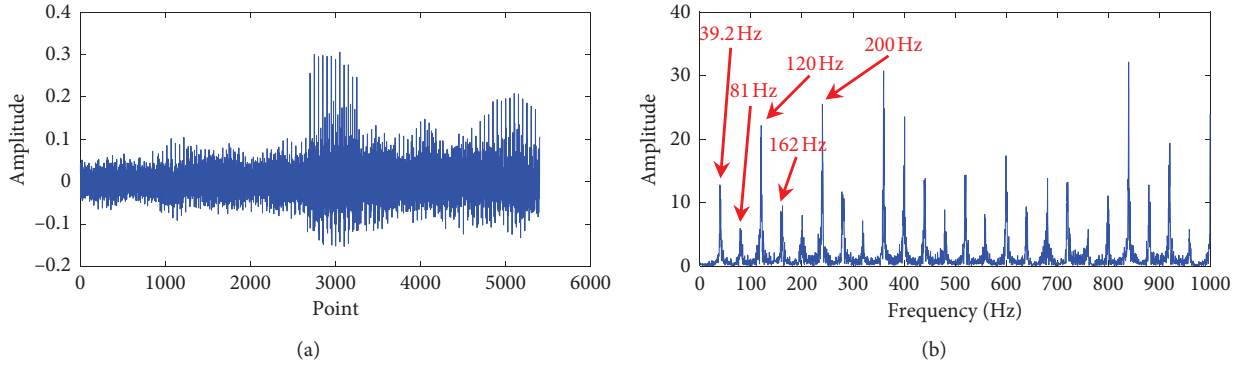

Figure 12: Results of MOMEDA: (a) time-domain waveform and (b) frequency-domain waveform.

amplitude of fault signals greatly, which is helpful for fault signal extraction under strong noise background.

5. Conclusion

The selection of filter length will affect the results of the CYCBD. Inappropriate filter length may cause the inaccurate extraction of fault signal. In this paper, the SOA is applied to the CYCBD, and the objective function constructed by the ratio of SNR to kurtosis is taken as the optimal target value. The optimal filter length is obtained by the iterative pattern.

The conclusion is as follows: if the filter length is too large or too small, CYCBD results will be distorted. In this study, the optimal filter length is adaptive determined by using CYCBD-SOA. The accuracy of the proposed method is verified by the periodic pulse extraction of the simulation signal. Meanwhile, CYCBD-SOA is successfully applied to bearing fault diagnosis. The crack fault of the outer ring of the bearing is obvious, and fault frequency 40 Hz and its

integer multiples can be extracted. By comparing the CYCBD-SOA with MCKD and MOMEDA in the test vibration signal, the reliability of the proposed method is verified.

Data Availability

The data used to support the findings of this study have not been made available because they are confidential.

Conflicts of Interest

The authors declare no conflicts of interest.

Authors' Contributions

Qianqian Zhang and Haochi Pan conceived and designed the experiments; Fujing Xu performed the experiments; Yulong Wu processed the data; Qiuxia Fan and Haochi Pan programed the algorithm; Qianqian Zhang wrote the paper. All authors have read and approved the final manuscript.

Acknowledgments

This work was supported in part by the Shanxi Provincial Natural Science Foundation of China (201901D211120), in part by the Shanxi Provincial Natural Science Foundation of China (201801D221339), in part by Shanxi Provincial Scientific Research Project of Returnees Studying Abroad (2020-007), and in part by the National Natural Science Foundation of China (61903240).

References

[1] J. Zhang, Y. Sun, L. Guo, H. Gao, X. Hong, and H. Song, "A new bearing fault diagnosis method based on modified convolutional neural networks," *Chinese Journal of Aeronautics*, vol. 33, no. 2, pp. 439–447, 2020.

[2] Y. Tan, L. Guo, H. Gao, and L. Zhang, "Deep coupled joint distribution adaptation network: a method for intelligent fault diagnosis between artificial and real damages," *IEEE Transactions on Instrumentation and Measurement*, vol. 70, pp. 1–12, 2021.

[3] Z. Wang, W. Zhao, W. Du, N. Li, and J. Wang, "Data-driven fault diagnosis method based on the conversion of erosion operation signals into images and convolutional neural network," *Process Safety and Environmental Protection*, vol. 149, pp. 591–601, 2021.

[4] J. Wang, G. Du, Z. Zhu, C. Shen, and Q. He, "Fault diagnosis of rotating machines based on the EMD manifold," *Mechanical Systems and Signal Processing*, vol. 135, Article ID 106443, 2020.

[5] Y. Sun, S. Li, and X. Wang, "Bearing fault diagnosis based on EMD and improved Chebyshev distance in SDP image," *Measurement*, vol. 176, no. 17, Article ID 109100, 2021.

[6] H. Shi, J. Guo, Z. Yuan, Z. Liu, M. Hou, and J. Sun, "Incipient fault detection of rolling element bearings based on deep EMD-PCA algorithm," *Shock and Vibration*, vol. 2020, Article ID 8871433, 17 pages, 2020.

[7] J. Li and J. Zhang, "Adaptive multiscale noise control enhanced stochastic resonance method based on modified EEMD with its application in bearing fault diagnosis," *Shock and Vibration*, vol. 2016, Article ID 1485412, 13 pages, 2016.

[8] H. Li, T. Liu, W. Xing et al., "Application of EEMD and improved frequency band entropy in bearing fault feature extraction," *ISA Transactions*, vol. 88, 2018.

[9] Z. Wang, J. Zhou, J. Wang et al., "A novel fault diagnosis method of gearbox based on maximum kurtosis spectral entropy deconvolution," *IEEE Access*, vol. 7, Article ID 29520, 2019.

[10] S. Ning, Z. Han, Z. Wang et al., "Application of sample entropy based LMD-TFPF de-noising algorithm for the gear transmission system," *Entropy*, vol. 18, no. 11, pp. 1–12, 2016.

[11] Z. Wang, G. He, W. Du et al., "Application of parameter optimized variational mode decomposition method in fault diagnosis of gearbox," *IEEE Access*, vol. 7, Article ID 44871, 2019.

[12] H. Li, T. Liu, X. Wu et al., "An optimized VMD method and its applications in bearing fault diagnosis," *Measurement*, vol. 166, Article ID 108185, 2020.

[13] Z. Wang, N. Yang, N. Li, W. Du, and J. Wang, "A new fault diagnosis method based on adaptive spectrum mode extraction," *Structural Health Monitoring*, Article ID 147592172098694, 2021.

[14] M. Buzzoni, J. Antoni, and G. D'Elia, "Blind deconvolution based on cyclostationarity maximization and its application to fault identification," *Journal of Sound and Vibration*, vol. 432, pp. 569–601, 2018.

[15] Z. Wang, J. Zhou, Y. Lei, and W. Du, "Bearing fault diagnosis method based on adaptive maximum cyclostationarity blind deconvolution," *Mechanical Systems and Signal Processing*, vol. 162, Article ID 108018, 2022.

[16] B. Zhang, Y. Miao, J. Lin, and Y. Yi, "Adaptive maximum second-order cyclostationarity blind deconvolution and its application for locomotive bearing fault diagnosis," *Mechanical Systems and Signal Processing*, vol. 158, Article ID 107736, 2021.

[17] R. Wiggins, "Minimum entropy deconvolution," *Geoexploration*, vol. 9, no. 16, pp. 21–35, 1978.

[18] J. Li, J. Jiang, X. Fan et al., "A new method for weak fault feature extraction based on improved MED," *Shock and Vibration*, vol. 2018, Article ID 9432394, 11 pages, 2018.

[19] Y. Cheng, N. Zhou, W. Zhang, and Z. Wang, "Application of an improved minimum entropy deconvolution method for railway rolling element bearing fault diagnosis," *Journal of Sound and Vibration*, vol. 425, pp. 53–69, 2018.

[20] G. L. Mcdonald, Q. Zhao, and M. J. Zuo, "Maximum correlated Kurtosis deconvolution and application on gear tooth chip fault detection," *Mechanical Systems and Signal Processing*, vol. 33, pp. 237–255, 2012.

[21] F. Wang, C. Liu, W. Su, Z. Xue, Q. Han, and H. Li, "Combined failure diagnosis of slewing bearings based on MCKD-CEEMD-ApEn," *Shock and Vibration*, vol. 2018, Article ID 6321785, 13 pages, 2018.

[22] L. Zhang, B. Cai, G. Xiong, J. Zhou, W. Tu, and Y. Yu, "Multistage fault feature extraction of consistent optimization for rolling bearings based on correlated kurtosis," *Shock and Vibration*, vol. 2020, Article ID 8846156, 16 pages, 2020.

[23] G. Mcdonald and Q. Zhao, "Multipoint optimal minimum entropy deconvolution and convolution fix: application to vibration fault detection," *Mechanical Systems and Signal Processing*, vol. 82, pp. 461–477, 2016.

[24] Z. Wang, W. Du, J. Wang et al., "Research and application of improved adaptive MOMEDA fault diagnosis method," *Measurement*, vol. 140, pp. 63–75, 2019.

[25] Y. Li, G. Cheng, and C. Liu, "Research on bearing fault diagnosis based on spectrum characteristics under strong noise interference," *Measurement*, vol. 169, no. 1, Article ID 108509, 2021.

[26] B. Chen, W. Zhang, D. Song et al., "Blind deconvolution assisted with periodicity detection techniques and its application to bearing fault feature enhancement," *Measurement*, vol. 159, Article ID 107804, 2020.

[27] X. Wang, X. Yan, and Y. He, "Weak fault detection for wind turbine bearing based on ACYCBD and IESB," *Journal of Mechanical Science and Technology*, vol. 34, no. 4, pp. 1399–1413, 2020.

[28] G. Dhiman and V. Kumar, "Seagull optimization algorithm: theory and its applications for large-scale industrial engineering problems," *Knowledge-Based Systems*, vol. 165, pp. 169–196, 2019.